universe

MDPI

Article

Radial Oscillations of the HESS J1731-347 Compact Object Imposing the Karmarkar Condition

Grigoris Panotopoulos

Departamento de Ciencias Físicas, Universidad de la Frontera, Casilla 54-D, Temuco 4811186, Chile; grigorios.panotopoulos@ufrontera.cl

Abstract: We model the light HESS J1731-347 compact object (of known stellar mass and radius) within Einstein's General Relativity, imposing the Karmarkar condition in gravity for anisotropic stars. The three free parameters of the analytic solution are determined by imposing the matching conditions at the surface of the star for objects of known stellar mass and radius. Finally, using well-established criteria, it is shown that the solution is compatible with all requirements for well-behaved and realistic solutions. Furthermore, we study the radial oscillation modes, and we compare them to the ones corresponding to an isotropic star modeled by the Tolman IV exact analytic solution obtained a long time ago. A comparison between the large frequency separations is made as well.

Keywords: compact objects; exact solutions; asteroseismology; radial oscillations

check for updates

Academic Editors: Polychronis Koliogiannis and Charalampos Moustakidis

Received: 17 February 2025
Revised: 25 April 2025
Accepted: 27 April 2025
Published: 1 May 2025

Citation: Panotopoulos, G. Radial Oscillations of the HESS J1731-347 Compact Object Imposing the Karmarkar Condition. *Universe* **2025**, *11*, 146. https://doi.org/10.3390/universe11050146

Copyright: © 2025 by the author. Licensee MDPI, Basel, Switzerland. This article is an open access article distributed under the terms and conditions of the Creative Commons Attribution (CC BY) license (https://creativecommons.org/licenses/by/4.0/).

1. Introduction

Thanks to Einstein's General Relativity (GR), which was formulated last century [1], we understand and describe a wide range of cosmological and astrophysical aspects. Einstein's gravity is considered worldwide to be both beautiful and successful, since many of its remarkable predictions have been confirmed. One can mention, for instance, the classical tests discussed in standard textbooks [2,3] as well as more recent ones after the historical LIGO's first direct detection of gravitational waves emitted from black hole binaries [4–6]. For a recent review on tests of GR, see, e.g., [7].

In spite of the mathematical elegance of GR, in most of the cases of interest, the study and analysis of realistic physical situations comprises a formidable task, due to the fact that Einstein's field equations are highly non-linear coupled partial differential equations. For that reason, the principle of superposition, which is valid in the theory of linear differential equations and which facilitates the task of obtaining the solution, does not apply in GR. Therefore, finding exact analytic solutions to the field equations of Einstein's gravity has always been an interesting and challenging topic, keeping researchers busy for decades. For exact known solutions to Einstein's field equations, see [8].

When studying stars, authors usually focus their attention on astrophysical objects made of matter viewed as a perfect fluid, where there is a unique pressure along all spatial dimensions, $p_r = p_\theta = p_\phi$. However, celestial bodies are not necessarily made of isotropic fluids. In fact, under certain conditions, the matter content of compact objects may become anisotropic. The review article of Ruderman [9] long time ago mentioned such a possibility: there, the author makes for the first time the observation that in very dense media anisotropies can be generated by interactions between relativistic particles. In the following years, the study on anisotropic relativistic stars received a boost by the subsequent work of [10]. Indeed, anisotropies may arise in many different physical situations, such as

phase transitions [11], pion condensation [12], or in the presence of type 3A super-fluid [13], to mention just a few.

Thanks to the work of [14], there is now a new and elegant method that permits us to construct anisotropic solutions starting from an already known seed isotropic solution. The so-called Minimal Geometric Deformation approach was originally introduced in [15] in the context of brane models [16,17], it has been extensively applied over the years, and it has been proven to be a powerful tool in the study of self-gravitating objects, such as relativistic stars or black holes [18–21], see also [22–26]. The aforementioned method was later extended in [27], and it was applied in [28], demonstrating its power and potential.

What is more, the author of [29] recently introduced the so-called complexity factor, which is a measure of the complexity of self-gravitating systems. Technically speaking, the complexity factor appears in the orthogonal splitting of the Riemann tensor. It is easy to see that it vanishes for isotropic spherical configurations or for fluid spheres characterized by homogeneous energy densities, but it may also vanish when the two terms containing density inhomogeneity and anisotropic pressure cancel each other. For articles on stars made of anisotropic matter within the complexity factor formalism, see, e.g., [30–40].

Another approach that allows us to find exact analytic interior solutions of relativistic stars is to impose the Karmarkar condition [41]. The method works equally well for compact objects made of isotropic and anisotropic matter. The strategy of the approach is the following: If one of the metric potentials is assumed, the Karmarkar condition allows us to obtain the other metric potential. After that, the energy density and the pressures of the fluid may be computed one by one, making use of the field equations. It is worth mentioning that within this approach, no equation-of-state (EoS) for the matter content is assumed. For an incomplete list of works obtaining interior solutions via the Karmarkar condition in gravity see e.g., [42–52].

As far as the inner structure of relativistic compact stars and the underlying EoS are concerned, the most massive pulsars [53–55] that have been observed over the last 15 years or so are putting constraints on different EoSs, since any mass-to-radius relationship that predicts a highest mass lower than the observed ones must be ruled out. In order to model a certain astronomical object, it would be advantageous to know both the stellar mass and radius. This is not always the case, since measuring the radius is much more difficult than measuring the stellar mass. As of today, there are some good strange quark star candidates, see, e.g., Table 5 of [56] or Table 1 of [57], and also the recently discovered massive pulsar PSR J0740+6620 [58–60] and the strangely light HESS J1731-347 compact object [61], where both the stellar mass and radius are known observationally. Based on modeling of the X-ray spectrum and a robust distance estimate from Gaia observations, the authors of [61] estimated the mass and the radius of the object to be $M = 0.77^{+0.20}_{-0.17} M_{\odot}$, $R = 10.40^{+0.86}_{-0.78} km$. Their estimate implies that this object is either the lightest neutron star known, or a 'strange star' with a more exotic equation of state. The recent observation of an exceptionally low mass compact object inside the supernovae remnant HESS J1731-347 challenges the standard neutron star formation models, and it has attracted a lot of attention among the nuclear physics community. Since it is one of the lightest and smallest astronomical objects ever observed, it raises many questions regarding its nature, and opens up the window for different possibilities to explain such a measurement [62].

Helioseismology and Asteroseismology in general, a research area that studies the oscillation modes of pulsating stars, is a powerful tool and a widely used technique to probe the inner structure of stars. The precise values of the frequency modes are very sensitive to the underlying physics and the corresponding equation-of-state of the dense matter content of compact objects. Therefore, studying the oscillations and computing the frequencies of the modes, we can learn more about the composition of compact objects, see,

e.g., [63–71] and references therein. Regarding excitation and detectability, numerous astrophysical mechanisms may excite oscillation modes of stars, such as tidal effects in binaries, starquakes caused by cracks during supernova explosions, magnetic reconfiguration, or any other form of instability [72–75].

The Kepler and CoRoT missions have already measured the oscillation spectra of solar-like, white dwarf, and red giant stars [76–79]. Current wave detectors, such as LIGO, cannot detect the radial oscillations studied here due to their low sensitivity at the kHz frequency range. However, the third-generation ground-based gravitational wave detectors are expected to have a much higher sensitivity (by an order of magnitude), such as the Cosmic Explorer [80] and the Einstein Telescope [81]. These detections could give us information related to neutron star masses, frequencies, tidal Love numbers, amplitudes of the modes, damping times, and moments of inertia. Upon comparison between accumulated experimental and observational data and well-accepted theoretical predictions, we should be able to probe and infer the EoS of dense matter.

Any exact analytic solution obtained within one of the aforementioned approaches must be physically relevant. In other words, it must be finite at the origin, well-behaved, and realistic, fulfilling all the well-established criteria discussed in the literature. Even better, it should be capable of modeling one or more of the observed stars of known mass and radius. The goal of the present study is twofold. First, we propose to model the HESS compact object assuming that it is made of anisotropic matter via the Karmarkar condition in gravity. Moreover, we shall show that the solution is well-behaved, capable of describing realistic astrophysical configurations. Furthermore, we shall study its radial oscillation modes, and make a comparison to the modes of its isotropic counterpart modeled via the Tolman IV solution [82,83].

In the present article, our work is organized as follows. After this introduction, in the next section, we briefly review relativistic compact objects assuming a non-vanishing factor of anisotropy, and we obtain an exact analytic solution. In Section 3, we summarize the usual criteria that ensure the existence of realistic solutions, we model the HESS compact object via the solution obtained in Section 2, and we demonstrate that it is capable of describing realistic astrophysical configurations. In the fourth section, we study the radial oscillation modes of the HESS compact object. For the sake of comparison, we also study radial oscillations of the isotropic counterpart. Finally, we conclude our work in the last section. Throughout the manuscript, we adopt the mostly positive metric signature, $\{-,+,+,+\}$, as well as geometrical units, in which both the speed of light in vacuum and Newton's constant are set to unity, $c = 1 = G$.

2. Anisotropic Relativistic Stars in Einstein's Gravity

2.1. Structure Equations for Fluid Spheres

When seeking interior solutions ($0 \leq r \leq R$, R being the radius of the star), the most general form of a static, spherically symmetric geometry in Schwarzschild-like coordinates, $\{t, r, \theta, \phi\}$, is given by

$$ds^2 = -e^{\nu}dt^2 + e^{\lambda}dr^2 + r^2(d\theta^2 + \sin^2\theta d\phi^2) \tag{1}$$

with $\nu(r), \lambda(r)$ being two independent functions of the radial coordinate. In the following section, we shall be working with the mass function, $m(r)$, which is defined by

$$e^{-\lambda} = 1 - \frac{2m}{r}. \tag{2}$$

In order to find solutions describing the hydrostatic equilibrium of compact objects, we have to integrate the Tolman–Oppenheimer–Volkoff equations [83,84]

$$m'(r) = 4\pi r^2 \rho(r) \tag{3}$$

$$p_r'(r) = -[\rho(r) + p_r(r)]\,\frac{\nu'(r)}{2} + \frac{2\Delta}{r} \tag{4}$$

$$\nu'(r) = 2\,\frac{m(r) + 4\pi r^3 p_r(r)}{r^2(1 - 2m(r)/r)} \tag{5}$$

where us usual a prime denotes differentiation with respect to r.

Next, anisotropic matter is described by a diagonal energy-momentum tensor of the form

$$T_a^b = Diag(-\rho, p_r, p_t, p_t) \tag{6}$$

where p_r, p_t are the radial and tangential pressure of matter, respectively, ρ is the energy density of the fluid, while the anisotropic factor is defined by

$$\Delta = p_t - p_r, \tag{7}$$

while in the case of stars made of isotropic matter, there is a unique pressure in both directions, $p_r = p_t$, and therefore $\Delta = 0$.

The Equations (3)–(5) are to be integrated imposing at the center of the star appropriate conditions

$$m(0) = 0, \quad p_r(0) = p_t(0) = p_c, \tag{8}$$

where p_c is the common central pressure, and therefore the anisotropic factor vanishes at the center of the star, $\Delta(0) = 0$. In addition, the following matching conditions must be satisfied at the surface of the object

$$p_r(R) = 0, \quad m(R) = M, \quad e^{\nu(R)} = 1 - 2\frac{M}{R}, \tag{9}$$

with M being the stellar mass, taking into account that the exterior vacuum solution ($r > R$) is given by the Schwarzschild geometry [85]

$$ds^2 = -(1 - 2M/r)dt^2 + (1 - 2M/r)^{-1}dr^2 + r^2(d\theta^2 + \sin^2\theta d\,\phi^2). \tag{10}$$

Finally, upon numerical integration, once the mass function and the radial pressure are known, the metric potential $\nu(r)$ is computed by

$$\nu(r) = \ln\left(1 - \frac{2M}{R}\right) + 2\int_R^r dx\,\frac{m(x) + 4\pi x^3 p_r(x)}{x^2(1 - 2m(x)/x)}. \tag{11}$$

2.2. Anisotropic Stars Imposing the Karmarkar Condition in Gravity

If the metric tensor satisfies the Karmarkar condition [41], it can represent an embedding class one spacetime

$$R_{1414} = \frac{R_{1212}R_{3434} + R_{1224}R_{1334}}{R_{2323}}, \tag{12}$$

with R_{2323} different than zero. This condition leads to a differential equation given by [42]

$$2\frac{\nu''}{\nu'} + \nu' = \frac{\lambda' e^{\lambda}}{e^{\lambda} - 1}. \tag{13}$$

If the function $\lambda(r)$ is given, upon integration we obtain the relationship between the metric potentials as follows [42]

$$e^{\nu} = \left(C_1 + \frac{1}{C_2}\int dr\sqrt{e^{\lambda}-1}\right)^2, \tag{14}$$

where C_1 and C_2 are arbitrary constants of integration. Equivalently, if the function $\nu(r)$ is given, the other metric potential upon integration is found to be

$$e^{\lambda} = 1 + \frac{B^2(\nu')^2 e^{\nu}}{4}, \tag{15}$$

where this time B is an arbitrary constant of integration.

In the discussion to follow we shall assume a metric potential of the form

$$\nu(r) = C + \left(\frac{r}{A}\right)^2, \tag{16}$$

which is characterized by two free constant parameters, A, C, and which is one of the potentials of the Krori–Barua ansatz [86]. It has been used among astronomers in the literature as it generates singularity-free solutions in general relativity [86]. Imposing the Karmarkar condition, the second metric potential is found to be

$$e^{\lambda} = 1 + \frac{B^2 r^2}{A^4} exp(C + (r/A)^2) \tag{17}$$

while the mass function is found to be

$$m(r) = \frac{B^2 r^3 exp(C + (r/A)^2)}{2[A^4 + B^2 r^2 exp(C + (r/A)^2)]} \tag{18}$$

Next, using the structure equations, the radial pressure and the energy density of the fluid may be computed, and they are given by

$$\rho(r) = \frac{B^2 exp(C + (r/A)^2)[3A^4 + 2A^2 r^2 + B^2 r^2 exp(C + (r/A)^2)]}{8\pi[A^4 + B^2 r^2 exp(C + (r/A)^2)]^2}, \qquad \rho_c = \rho(0) = \frac{3B^2 e^C}{8\pi A^4} \tag{19}$$

$$p_r(r) = \frac{2A^2 - B^2 exp(C + (r/A)^2)}{8\pi[A^4 + B^2 r^2 exp(C + (r/A)^2)]}, \qquad p_c = p_r(0) = \frac{2 - (B/A)^2 e^C}{8\pi A^2}, \tag{20}$$

where the central values p_c, ρ_c are found to be finite, while at the same time the radial pressure vanishes when

$$R = A\sqrt{-C + ln\left(\frac{2A^2}{B^2}\right)}, \tag{21}$$

which corresponds to the stellar radius. Finally, the anisotropy $\Delta(r)$ is found to be

$$\Delta(r) = \frac{[A^2 - B^2 exp(C + (r/A)^2)]^2 r^2}{8\pi[A^4 + B^2 r^2 exp(C + (r/A)^2)]^2}, \tag{22}$$

and the tangential pressure, $p_t = \Delta + p_r$, is computed to be

$$p_t(r) = \frac{A^4[2A^2 + r^2 - B^2 exp(C + (r/A)^2)]}{8\pi[A^4 + B^2 r^2 exp(C + (r/A)^2)]^2}. \tag{23}$$

Finally, the speed of sounds at constant entropy, $c_{s,r}, c_{s,t}$, and the relativistic adiabatic indices, Γ_r, Γ_t, are defined as

$$c_{s,i}^2 \equiv \left(\frac{dp_i}{d\rho}\right)_S = \frac{p_i'(r)}{\rho'(r)} \tag{24}$$

$$\Gamma_i \equiv c_{s,i}^2\left(1+\frac{\rho}{p_i}\right), \tag{25}$$

for both directions, namely radial (r) and tangential (t), $i = r, t$, and they are computed in terms of the known functions $p_r(r), p_t(r), \rho(r)$ and their derivatives.

3. Modeling the HESS Compact Object

3.1. Criteria for Realistic Solutions

Before we proceed with stellar modeling, we shall report here the requirements for well-behaved solutions capable of describing realistic astrophysical configurations. The well-established criteria discussed in the literature are the following:

- Causality, i.e., the speed of sound must be lower than the speed of light in vacuum

$$0 \leq c_s^2 \leq 1 \tag{26}$$

- Stability based on the relativistic adiabatic index, i.e., its mean value must be larger than a critical value

$$\langle\Gamma\rangle \geq \Gamma_{cr} \tag{27}$$

where the critical value is given by [87]

$$\Gamma_{cr} = \frac{4}{3} + \frac{19}{21}\frac{M}{R} \tag{28}$$

while the mean value is computed by [87]

$$\langle\Gamma\rangle = \frac{\int_0^R dr\,\Gamma(r)p(r)r^2e^{(\lambda+3\nu)/2}}{\int_0^R dr\,p(r)r^2e^{(\lambda+3\nu)/2}}. \tag{29}$$

- The energy conditions impose certain constraints on the stress-energy tensor of matter within a given theory of gravity. The acceptable conditions assumed for the energy-momentum tensor are as follows: weak energy condition (WEC), dominant energy condition (DEC), null energy condition (NEC), and strong energy condition (SEC), see for instance [88–90]. If ξ_μ and k_μ are arbitrary time-like and null vectors, respectively, then the conditions for the energy-momentum tensor are expressed with the following inequalities

$$T^{\mu\nu}\,\xi_\mu\,\xi_\nu \geq 0, \quad (WEC) \tag{30}$$

$$T^{\mu\nu}\,\xi_\mu\,\xi_\nu \geq 0 \text{ and } T^{\mu\nu}\,\xi_\mu \text{ is a non-spacelike vector}, \quad (DEC) \tag{31}$$

$$T^{\mu\nu}\,k_\mu\,k_\nu \geq 0, \quad (NEC) \tag{32}$$

$$T^{\mu\nu}\,\xi_\mu\,\xi_\nu - (1/2)T^\mu_\mu\,\xi^\nu\,\xi_\nu \geq 0. \quad (SEC) \tag{33}$$

In particular, in the case of isotropic fluids, the energy conditions require that [91,92]

$$\rho \geq 0, \qquad \rho + 3p \geq 0, \qquad \rho \pm p \geq 0. \tag{34}$$

while in the case of anisotropic fluids, the energy conditions take the form

$$\rho \geq 0, \qquad \rho + p_r + 2p_t \geq 0, \qquad \rho \pm p_i \geq 0, \quad i = r, t. \tag{35}$$

3.2. The HESS J1731-347 Object

Imposing the following matching conditions at the surface of the star, $r \to R$

$$p_r(R) = 0, \qquad m(R) = M, \qquad e^{\nu(R)} = 1 - 2\frac{M}{R} \tag{36}$$

we find the following values of the free parameters

$$A = 27.90km, \qquad B = 44.64km, \qquad C = -0.39 \tag{37}$$

considering stellar mass and radius $M = 0.77M_{\odot}$ and $R = 10.47km$, respectively. For those numerical values of A, B, C, the central values of the energy density and both pressures are found to be

$$\rho_c = 200.83\, MeV/fm^3, \qquad p_c = 10.13\, MeV/fm^3. \tag{38}$$

Furthermore, the relations between the energy density and both pressures are shown in the lower panel of Figure 1. The pressures increase with the energy density, which is the typical behavior of any equation-of-state. Since they seem to be almost linear, we make a comparison with a linear MIT bag model EoS, (extreme model SQSB40) [93], see the discussion below for more details on that model. The $p - \rho$ relation corresponding to the Tolman IV solution (see Section 4.2) is also included. What is more, since there is an analytic expression both for the stellar radius and the stellar mass in terms of the constant parameters A, B, C, we may generate the M-R relationships displayed in the upper panel of Figure 1. The red curve is a straight line corresponding to fixed B, C and varying A, whereas the blue curve is a non-linear function that is obtained fixing A, C and varying B or fixing A, B and varying C. The two curves meet at the point that represents the HESS compact object modeled in the present work. Finally, using the $p - \rho$ relationship one may solve the TOV equations numerically to obtain the M-R relationship shown in the middle panel of Figure 1. It does not come as a surprise that it looks very similar to the M-R profiles of strange quark stars. The $M - R$ profiles of the quark star and of the HESS object modeled via the Tolman solution, too, are shown for comparison reasons. We have included the allowed stellar mass and radius range of the HESS compact object as well.

We comment in passing that although it is not obvious, it turns out that the solution obtained here is unique. It is not difficult to verify this numerically. One of the three matching conditions may be used to express the parameter C in terms of the other two. Then, the other two matching conditions imply certain relations between A and B. One may draw the contour plots, and observe that the two curves meet at a single point.

Next, all the quantities of interest, such as sound speed, factor of anisotropy, etc., versus r are displayed in the Figures 2 and 3 below. In particular, Figure 3 shows the speed of sound and the relativistic adiabatic index, in both directions, versus r. In the lower panel of Figure 2, it is observed that the tangential pressure is larger than the radial one, and so the anisotropic factor is positive. For the sake of comparison, we show in the same plot (upper panel of Figure 2) the energy density and the pressure of a quark star made of isotropic matter. The red color corresponds to the analytic solution discussed here, whereas the black color corresponds to the quark star assuming a linear EoS of the form (extreme model SQSB40) [93]

$$p_q = k(\rho_q - \rho_0), \tag{39}$$

where the parameters k, ρ_0 take the numerical values [93]

$$k = 0.324, \qquad \rho_0 = 3.06 \times 10^{17} kg/m^3. \tag{40}$$

for $m_s = 100MeV, \alpha_c = 0.6$ and $B = 40MeV/fm^3$, with m_s being the mass of the s quark, α_c being the strong coupling constant, and B being the bag constant [93]. For those values, and for a central pressure $p_{q,c} = 1.275\,\rho_0$, the mass and radius of the quark star are found to be $M_q = 0.79M_\odot, R_q = 10.38km$. We see that the functions $p(r), \rho(r)$ corresponding to the numerical solution lie very close to the ones corresponding to the analytic solution. Therefore, a quark star made of isotropic matter, too, may model the HESS compact object for very similar energy density and pressure.

According to our results, since both energy density and pressures are positive, and $\rho > p_i, i = r, t$ all the energy conditions are fulfilled, while at the same time causality is not violated. Moreover, both the pressure and the energy density of the fluid are finite at the center of the star, and they monotonically decrease with the radial coordinate. Finally, since $\Gamma > \Gamma_{cr}$, we conclude that the stability criterion is met as well.

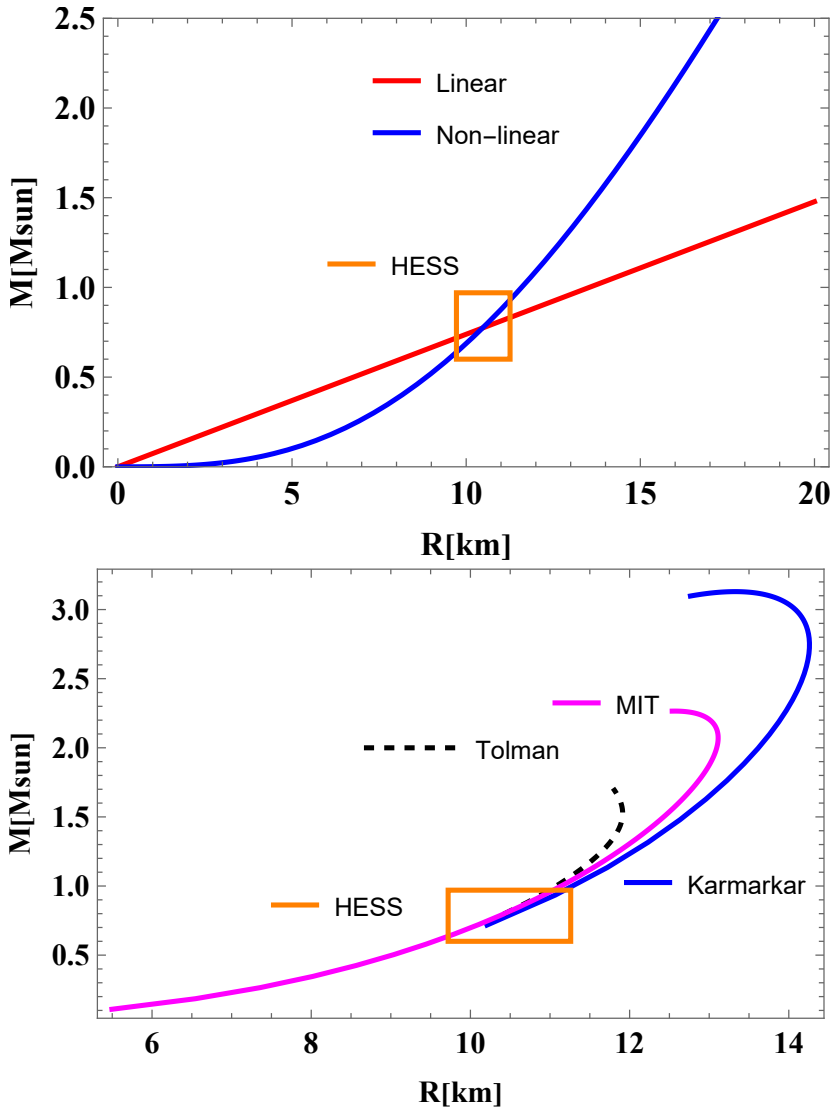


Figure 1. *Cont.*

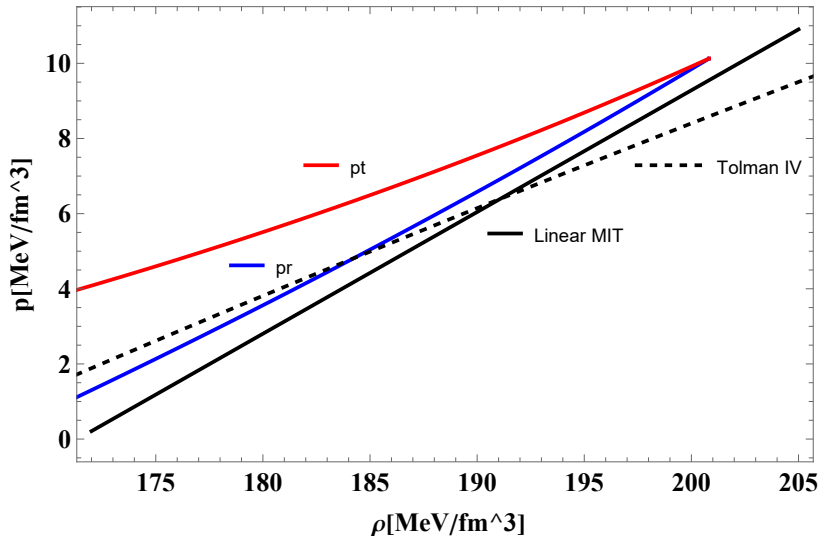


Figure 1. Mass-to radius-relationships (upper and middle panels), and pressure versus energy density $p - \rho$ (lower panel) for the solution discussed in this work. In the upper panel, the analytic expressions for the stellar mass and radius were used, whereas in the middle panel, the TOV equations were integrated numerically using the $p - \rho$ relationship. For comparison reasons the M-R relationships corresponding to the MIT bag model, as well as the Tolman IV solution, are shown as well. The allowed range of the HESS compact object, too, is included. In the lower panel, a comparison is made between the radial and tangential pressure versus energy density for the analytic solution discussed in this work, the linear MIT EoS of the model SQSB40, and the $p - \rho$ relationship of the Tolman IV solution.

It is worth noticing that the solution found here is based on the use of the Karmarkar condition and in the particular choice of the metric potential. Following another approach or choosing another metric potential will lead to different expressions for the quantities of interest and different numerical values of the free parameters of the solution. Furthermore, if another approach is adopted (for example one may assume a concrete EoS and a certain relationship between energy density and anisotropic factor or a certain mass function), the new solution does not have to satisfy the Karmarkar condition.

Furthermore, as a conjectural corollary, let us argue an analogy to the proposal by [94–96] of the so-called two-family scenario: Two distinct families of compact objects could coexist in nature. The first family (hadronic neutron stars) could explain some observations, while the second family (strange quark stars) could explain some others. According to that scenario, objects characterized by small stellar masses and radii are hadronic, whereas objects characterized by large stellar masses and radii are made of quark matter. Given the TOV results shown in the middle panel of Figure 1, since according to the blue curve $M_{max} \approx 3M_{\odot}$, it can be confirmed that the obtained $M - R$ relationship is compatible with the original Drago proposal. It must be emphasized, however, that when anisotropies are present, like in the present study, things can and will change compared to stars made of isotropic matter, since when $\Delta > 0$ the EoS can support a higher maximum stellar mass.

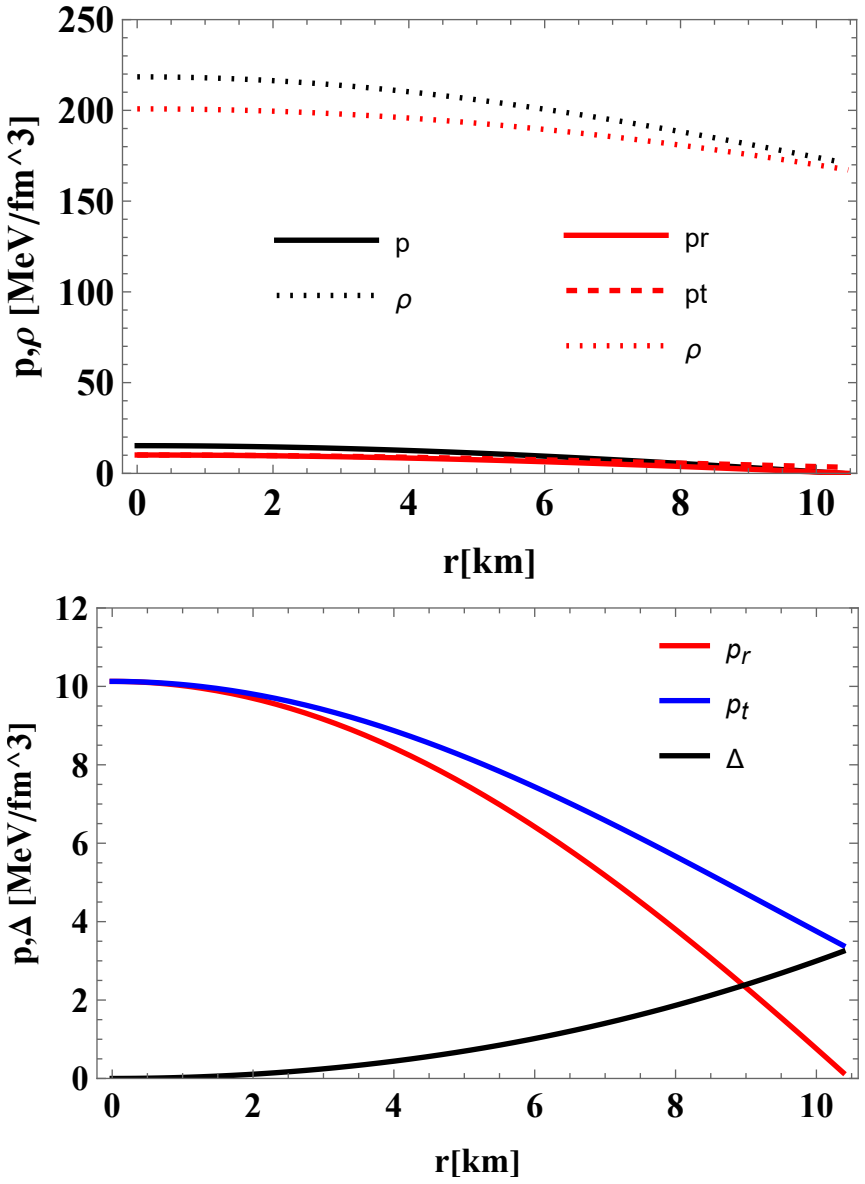


Figure 2. Energy density and pressures (upper panel), and pressures and anisotropic factor (lower panel) versus radial coordinate in km, for the HESS compact object. The radial pressure vanishes at $r = R$, while the anisotropic factor vanishes at the origin, $\Delta(0) = 0$. In the upper panel, the red curves correspond to the analytic solution discussed here, whereas the black curves correspond to a numerical solution assuming the MIT bag model SQSB40 for quark matter.

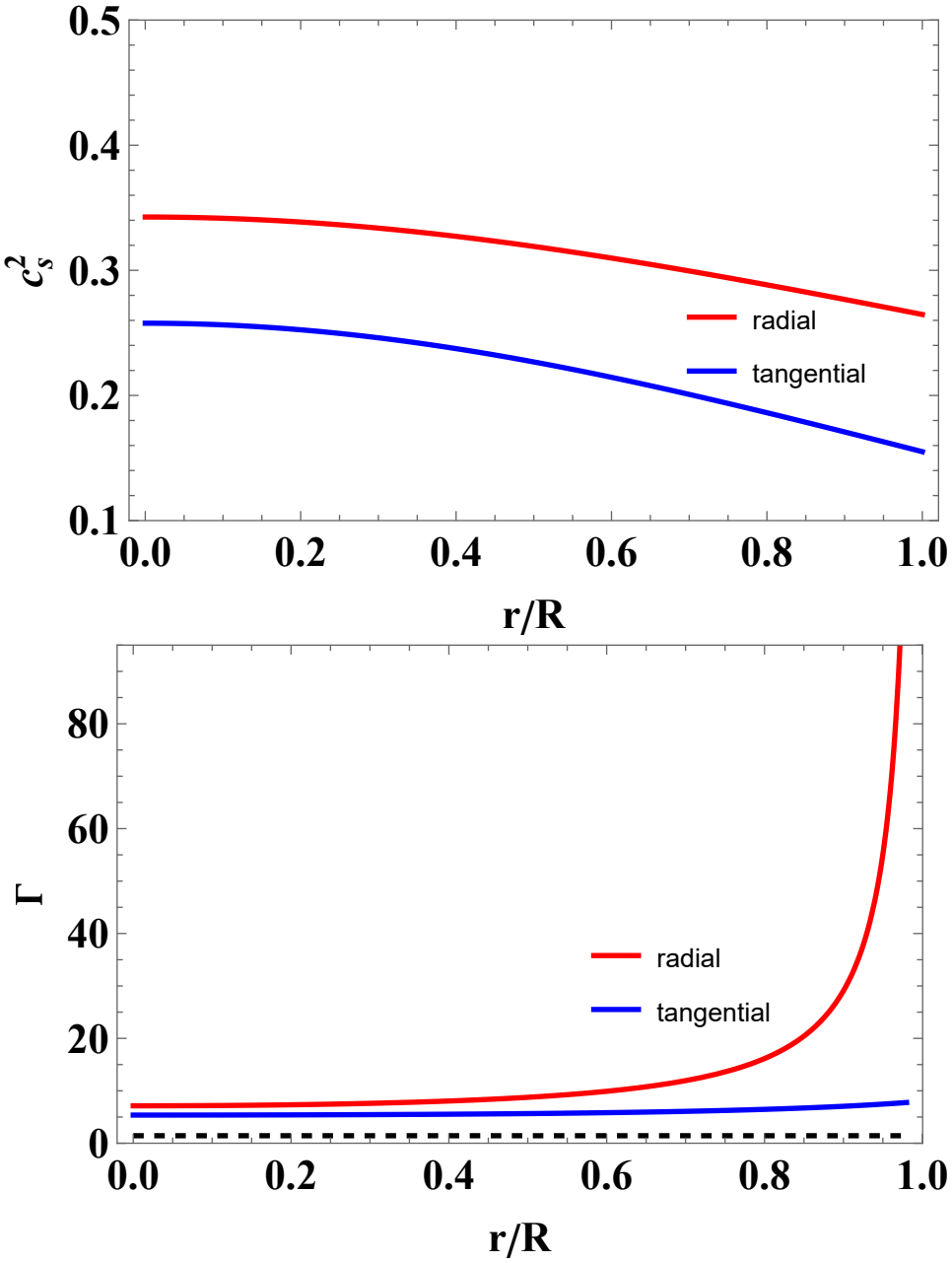


Figure 3. Speed of sound (upper panel) and relativistic adiabatic index (lower panel) versus dimensionless radial coordinate, r/R, for the HESS compact object. The horizontal dashed line corresponds to the critical value of $\Gamma_{cr} = 1.43$. The red curves correspond to the radial direction, while the blue curves correspond to the tangential direction.

4. Radial Oscillation Modes of Relativistic Stars

4.1. Equations for Perturbations

Assuming a system with radial motion only, Einstein's field equations may be used to compute the spectra of a static equilibrium structure. Considering the radial displacement Δr and the pressure perturbation ΔP as small perturbations to the background solution, the dimensionless quantities $\xi \equiv \Delta r/r$ and $\eta \equiv \Delta P/P$ are found to satisfy a first order system of coupled differential equations as follows [97,98]

$$\xi'(r) = -\frac{1}{r}\left(3\xi + \frac{\eta}{\Gamma}\right) - \frac{P'(r)}{P+\rho}\xi(r), \tag{41}$$

$$\eta'(r) = \xi\left[\omega^2 r(1+\rho/P)e^{\lambda-\nu} - \frac{4P'(r)}{P} - 8\pi(P+\rho)re^{\lambda} + \frac{r(P'(r))^2}{P(P+\rho)}\right] + \eta\left[-\frac{\rho P'(r)}{P(P+\rho)} - 4\pi(P+\rho)re^{\lambda}\right], \tag{42}$$

with ω being the frequency oscillation mode. The above equations for perturbations allow us to study the radial oscillation modes of stars made of isotropic matter. In the case of anisotropic stars, there are some additional terms that are proportional to the anisotropic factor, and therefore the linear system of coupled perturbations reads [99]

$$\xi'(r) = -\frac{1}{r}\left(3\xi + \frac{\eta}{\Gamma}\right) - \left(\frac{P'(r)}{P+\rho} + \frac{2\Delta}{rP\Gamma}\right)\xi(r), \tag{43}$$

$$\eta'(r) = \xi\left[\omega^2 r(1+\rho/P)e^{\lambda-\nu} - \frac{4P'(r)}{P} - 8\pi(P+\rho)re^{\lambda}\frac{P+\Delta}{P} + \frac{8\Delta}{rP} + \frac{r(P'(r))^2}{P(P+\rho)}\right] + \eta\left[-\frac{\rho P'(r)}{P(P+\rho)} - 4\pi(P+\rho)re^{\lambda}\right], \tag{44}$$

where now P, Γ are the radial quantities, $P(r) = p_r(r), \Gamma(r) = \Gamma_r(r)$.

Those two coupled differential equations, Equations (43) and (44), are supplemented with two boundary conditions: one at the center, where $r = 0$, and another at the surface, where $r = R$. The Equation (43) must be finite at the center, and therefore, the boundary condition at the origin requires that

$$\eta = -3\Gamma\xi \tag{45}$$

must be satisfied. Moreover, the equation Equation (44) must be finite at the surface and hence

$$\eta = \xi\left[-4 + (1-2M/R)^{-1}\left(-\frac{M}{R} - \frac{\omega^2 R^3}{M}\right)\right] \tag{46}$$

must be satisfied, where M and R correspond to the mass and radius of the star, respectively. The frequencies are computed by

$$\nu = \frac{\omega}{2\pi} = \frac{s\,\omega_0}{2\pi}\ \text{(kHz)}, \tag{47}$$

where s is a dimensionless number, while $\omega_0 \equiv \sqrt{M/R^3}$.

Those equations represent the Sturm–Liouville eigenvalue equations for ω. The solutions provide the discrete eigenvalues ω_n^2 and can be ordered as

$$\omega_0^2 < \omega_1^2 < ... < \omega_n^2,$$

where n is the number of nodes of the corresponding eigenmode for a star of a given mass and radius.

We use the shooting method analysis, where one starts the integration for a trial value of ω^2 and a given set of initial values that satisfy the boundary condition at the center. We integrate towards the surface, and the discrete values of ω^2 for which the boundary conditions are satisfied correspond to the eigenfrequencies of the radial perturbations.

Finally, one commonly used indicator is the so called large frequency separation

$$\Delta\nu_n = \nu_{n+1} - \nu_n, \quad n = 0, 1, 2, 3, ... \tag{48}$$

which can be easily computed once the spectrum is known. In other words, it is the difference between consecutive modes, and it can be shown to relate to stellar mass and radius [100–102].

4.2. Tolman IV Solution

Before we proceed with the discussion of the numerical results regarding the frequencies and corresponding eigenfunctions of the HESS compact object, let us briefly review the Tolman IV solution [83]. Among the hundreds of exact analytic solutions to the field equations of GR, the Tolman solution is one of the few solutions with physical meaning, in the sense that there is a well defined stellar mass and radius, subluminous speed of sound, while at the same time the energy density and the pressure of the fluid are positive definite, regular at the origin, and monotonically descreasing functions of the radial coordinate throughout the star [82].

We may start assuming a metric potential of the form

$$e^{\lambda(r)} = \frac{1+2(r/a)^2}{[1-(r/r_0)^2][1+(r/a)^2]}. \tag{49}$$

Next, using the definition of the mass function as well as the first structure equation, the energy density and the mass function are computed to be

$$\rho(r) = \frac{1}{8\pi r_0^2}\frac{6r^4+(7a^2+2r_0^2)r^2+3a^4+3a^2r_0^2}{(a^2+2r^2)^2}, \tag{50}$$

$$m(r) = \frac{r^3}{2r_0^2}\frac{r^2+a^2+r_0^2}{a^2+2r^2}. \tag{51}$$

Finally, making use of the other two structure equations, the pressure of the fluid and the other metric potential, $\nu(r)$, are found to be [82]

$$p(r) = \frac{1}{8\pi r_0^2}\frac{r_0^2-a^2-3r^2}{2r^2+a^2}, \tag{52}$$

$$e^{\nu(r)} = b^2[1+(r/a)^2]. \tag{53}$$

Clearly, the solution is characterized by three constant parameters a, b, r_0. As a check, it is straightforward to verify that all structure equations are satisfied. We see that both the pressure and the energy density remain finite at the center of the star, while at the same time the pressure becomes zero at a finite radius R, which is found to be

$$R = \frac{r_0}{\sqrt{3}}\sqrt{1-\frac{a^2}{r_0^2}}. \tag{54}$$

Finally, the speed of sound, c_s, and the relativistic adiabatic index, Γ, for the Tolman IV solution are found to be

$$c_s^2(r) = \frac{p'(r)}{\rho'(r)} = \frac{2r^2+a^2}{2r^2+5a^2} \tag{55}$$

$$\Gamma(r) = c_s^2\left(1+\frac{\rho}{p}\right) = 2\frac{(r^2+a^2)(2r_0^2+a^2)}{(2r^2+5a^2)(r_0^2-a^2-3r^2)}. \tag{56}$$

Recently, it was shown in [103] that the Tolman IV solution is capable of modeling the HESS compact object, provided that the latter is isotropic, if the parameters of the solution take the numerical values

$$a = 25.07km, \quad r_0 = 30.89km, \quad b = 0.81 \tag{57}$$

leading to a stellar mass of $M = 0.80M_{\odot}$ and a stellar radius of $R = 10.42km$.

4.3. Discussion of the Results

The frequencies of the 8 lowest modes (fundamental, $n = 0$ and seven excited modes, $n = 1, 2, ..., 7$) are shown in Table 1 both for the anisotropic HESS compact object (modeled here via the Karmarkar condition) and the isotropic HESS compact object (modeled in [103] via the Tolman solution) of very similar stellar mass and radius. Moreover, the large frequency separations are displayed in Figure 4, while the corresponding eigenfunctions $\xi(r), \eta(r)$ are shown in Figure 5. We observe that the large difference separations tend to a certain constant at highly excited modes, in agreement to the asymptotic theory [100]

$$\Delta\nu \approx \left(2\int_0^R \frac{dr}{c_s(r)}\right)^{-1}, \tag{58}$$

and so a larger speed of sound implies a higher constant frequency separation.

Table 1. Frequencies (in kHz) of radial oscillation modes both for isotropic and anisotropic stars. We have considered $M = 0.8M_{\odot}$ and $R = 10.42km$ in the case of the isotropic object, and $M = 0.77M_{\odot}$ and $R = 10.47km$ in the case of the anisotropic star.

Mode Order *n*	**Isotropic Star**	**Anisotropic Star**
0	4.48	5.81
1	10.27	12.62
2	15.76	19.20
3	21.17	25.72
4	26.55	32.22
5	31.93	38.72
6	37.29	45.20
7	42.65	51.68

The radial profiles $\xi(r), \eta(r)$ for isotropic and anisotropic stars are qualitatively very similar, the main difference being the value of the η function at the origin, due to the fact that the relativistic adiabatic index is different from one model to another. Here we have displayed the eigenfunctions of the isotropic star. We notice that the radial profiles of the perturbations exhibit the typical behavior observed in any Sturm–Liouville problem, namely the number of zeros of the eigenfunctions equals the value of the overtone number $n = 0, 1, 2, ...$ Our findings show that the spectrum of the anisotropic object is characterized by higher frequencies, and also by larger constant frequency separation at highly excited modes, $\Delta\nu^{iso} \approx 5.36$ kHz in the case of isotropic star, and $\Delta\nu^{aniso} \approx 6.48$ kHz in the case of anisotropic star. Finally, for the sake of comparison, in Figure 6 we have displayed the speed of sounds versus the normalized radial coordinate both for the isotropic and the anisotropic HESS compact object. The dashed curve corresponds to the isotropic star (Tolman IV solution), while the solid curve corresponds to the radial sound speed of the anisotropic object (via Karmarkar condition in gravity). Both are finite, monotonic functions of r within the range $(0, 1)$. In the case of isotropic star c_s^2 increases, whereas in the case of the anisotropic star the sound speed decreases with r. The speed of sound of the

anisotropic object lies above the sound speed of its isotropic counterpart, which explains why $\Delta\nu^{aniso} > \Delta\nu^{iso}$.

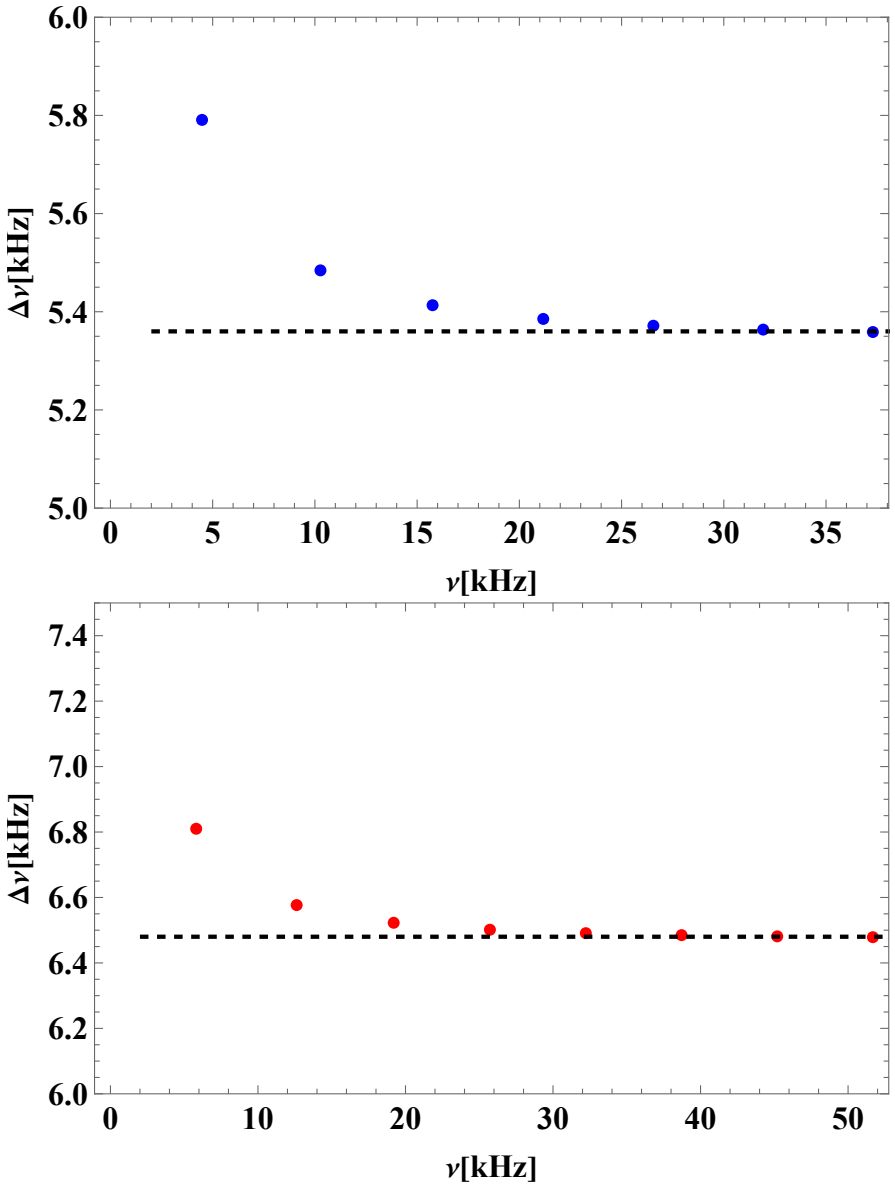


Figure 4. Large frequency separations for isotropic star (Tolman IV solution, upper panel) and anisotropic object (via Karmarkar condition, lower panel) versus frequency for the HESS compact object. At higher excited modes the separation tends to a constant value, $\Delta\nu^{iso} \approx 5.36$ kHz in the case of isotropic star, and $\Delta\nu^{aniso} \approx 6.48$ kHz in the case of anisotropic star.

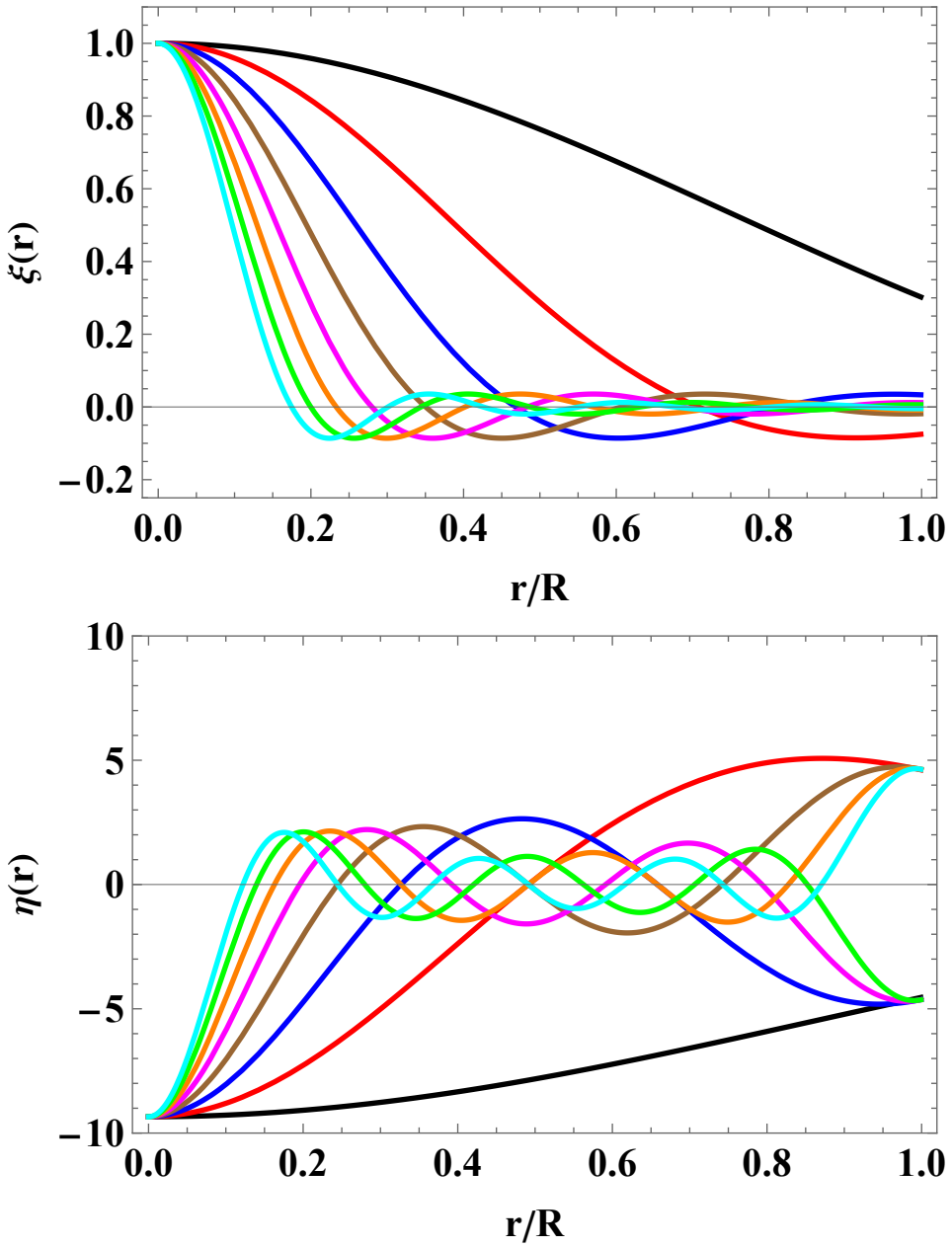


Figure 5. Radial profiles of eigenfunctions versus normalized radial coordinate, r/R for the fundamental mode, $n = 0$, as well as seven excited modes, $n = 1, 2, ...7$. The upper panel corresponds to the $\xi(r)$ function, while the lower panel to $\eta(r)$ function.

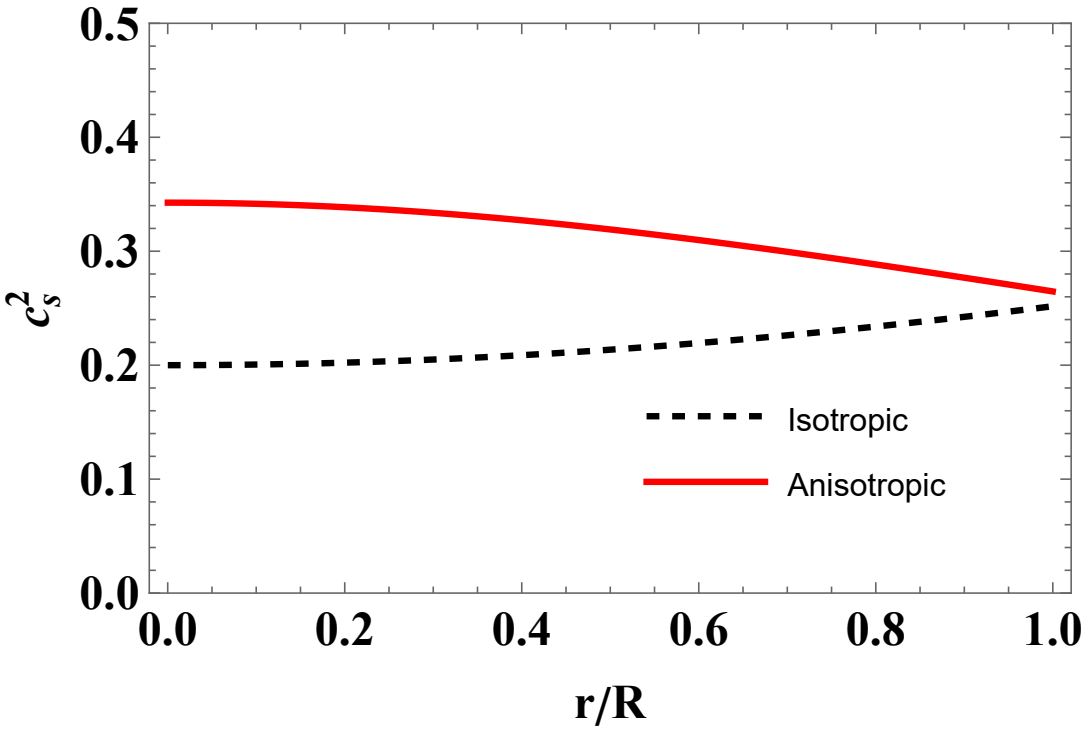


Figure 6. Speed of sound versus radial coordinate for anisotropic star (red solid curve) and isotropic object (black dashed curve).

5. Concluding Remarks

To summarize our work, in this article, we proposed to model the HESS J1731-347 compact object (of known mass and radius) assuming that the star is made of anisotropic matter and imposing the Karmarkar condition in gravity, and we studied its radial oscillation modes. First, the general description of relativistic stars made of anisotropic matter within Einstein's gravity was reviewed. Next, we obtained an exact analytic solution via the Karmarkar condition for anisotropic stars. The three free parameters of the solution were determined by imposing the appropriate matching conditions at the surface of the star of known mass and radius. Although the system of algebraic equations is non-linear, we found a unique solution.

The mass-to-radius profiles as well as the $p - \rho$ relationships were shown. Then, the behavior of the solution was displayed graphically. The quantities of interest, such as relativistic adiabatic index, energy density, anisotropic factor, speed of sound, etc., were found to be finite at the origin and at the same time smooth, continuous functions of the radial coordinate throughout the star. Moreover, well-established criteria, such as energy conditions, causality, and stability based on the adiabatic relativistic index, were shown to be fulfilled. Since the energy density and both pressures were found to be positive, and also the energy density was higher than both radial and tangential pressure, all four energy conditions are satisfied. For comparison reasons we showed in the same figure the energy density and the pressures for the anisotropic HESS object as well as its isotropic counterpart. It is confirmed that our proposal of a Karmarkar solution to the HESS object qualitatively mimics to a strange quark star. One limitation of our Karmarkar solution, however, is that other constraints on neutron stars are not being considered in the present work. Massive radio pulsars, the NICER, the gravitational waves GW170817 and GW190425 from neutron star mergers, and their electromagnetic counterparts kilonova AT2017gfo and gamma ray bursts 170817A are being used to put constraints on neutron stars, see e.g., [104–106]. Finally, given the new TOV results shown in the middle panel of Figure 1, since according

to the blue curve $M_{max} \approx 3M_{\odot}$, it can be confirmed that the obtained $M - R$ relationship is compatible with the original Drago proposal.

Next, regarding the spectrum of pulsating stars, we solved the equations for the perturbations imposing appropriate boundary conditions, and we computed (i) the frequencies of the 8 lowest modes, (ii) the corresponding eigenfunctions, and (iii) the large frequency separations. Finally, for the sake of comparison, we also studied the radial oscillation modes of the same object modeled via the Tolman IV solution for isotropic objects. Our findings indicate that the spectrum of the star made of anisotropic matter is characterized by higher frequencies, in agreement with the fact that its speed of sound was found to be higher than that of its isotropic counterpart.

Funding: This research received no external funding.

Data Availability Statement: This is a theoretical work, and so no data have been reported here.

Acknowledgments: The author wishes to thank the anonymous referees for useful comments and suggestions.

Conflicts of Interest: The author declares no conflicts of interest.

References

1. Einstein, A. The Field Equations of Gravitation. *Sitzungsber. Preuss. Akad. Wiss. Berlin Math. Phys.* **1915**, *1915*, 844–847.
2. Weinberg, S. *Gravitation and Cosmology: Principles and Applications of the General Theory of Gravitation*; John Wiley and Sons: Hoboken, NJ, USA, 1972.
3. Meisner, C.W.; Thorne, K.S.; Wheeler, J.A. *Gravitation*; Princeton University Press: Princeton, NJ, USA, 1973.
4. Abbott, B.P. et al. [LIGO Scientific and Virgo] Observation of Gravitational Waves from a Binary Black Hole Merger. *Phys. Rev. Lett.* **2016**, *116*, 061102. [CrossRef]
5. Abbott, B.P. et al. [LIGO Scientific and Virgo] GW151226: Observation of Gravitational Waves from a 22-Solar-Mass Binary Black Hole Coalescence. *Phys. Rev. Lett.* **2016**, *116*, 241103. [CrossRef] [PubMed]
6. Abbott, B.P. et al. [LIGO Scientific and VIRGO] GW170104: Observation of a 50-Solar-Mass Binary Black Hole Coalescence at Redshift 0.2. *Phys. Rev. Lett.* **2017**, *118*, 221101; Erratum in *Phys. Rev. Lett.* **2018**, *121*, 129901. [CrossRef]
7. Asmodelle, E. Tests of General Relativity: A Review. *arXiv* **2017**, arXiv:1705.04397.
8. Stephani, H.; Kramer, D.; Maccallum, M.; Hoenselaers, C.; Herlt, E. *Exact Solutions of Einstein's Field Equations*; Cambridge University Press: Cambridge, UK, 2003.
9. Ruderman, R. Pulsars: Structure and dynamics. *Ann. Rev. Astron. Astrophys.* **1972**, *10*, 427. [CrossRef]
10. Bowers, R.L.; Liang, E.P.T. Anisotropic Spheres in General Relativity. *Astrophys. J.* **1974**, *188*, 657. [CrossRef]
11. Sokolov, A.I. Phase transitions in a superfluid neutron liquid. *JETP* **1980**, *79*, 1137.
12. Sawyer, R.F. Condensed π^- Phase in Neutron Star Matter. *Phys. Rev. Lett.* **1972**, *29*, 823. [CrossRef]
13. Kippenhahn, R.; Weigert, A. *Stellar Structure and Evolution*; Springer: Berlin, Germany, 1990.
14. Ovalle, J. Decoupling gravitational sources in general relativity: From perfect to anisotropic fluids. *Phys. Rev. D* **2017**, *95*, 104019. [CrossRef]
15. Ovalle, J. Searching exact solutions for compact stars in braneworld: A Conjecture. *Mod. Phys. Lett. A* **2008**, *23*, 3247–3263. [CrossRef]
16. Randall, L.; Sundrum, R. A Large mass hierarchy from a small extra dimension. *Phys. Rev. Lett.* **1999**, *83*, 3370–3373. [CrossRef]
17. Randall, L.; Sundrum, R. An Alternative to compactification. *Phys. Rev. Lett.* **1999**, *83*, 4690–4693. [CrossRef]
18. Estrada, M.; Tello-Ortiz, F. A new family of analytical anisotropic solutions by gravitational decoupling. *Eur. Phys. J. Plus* **2018**, *133*, 453. [CrossRef]
19. Morales, E.; Tello-Ortiz, F. Compact Anisotropic Models in General Relativity by Gravitational Decoupling. *Eur. Phys. J. C* **2018**, *78*, 841. [CrossRef]
20. Estrada, M.; Prado, R. The Gravitational decoupling method: The higher dimensional case to find new analytic solutions. *Eur. Phys. J. Plus* **2019**, *134*, 168. [CrossRef]
21. Ovalle, J.; Casadio, R.; Rocha, R.d.; Sotomayor, A.; Stuchlik, Z. Black holes by gravitational decoupling. *Eur. Phys. J. C* **2018**, *78*, 960. [CrossRef]
22. Ovalle, J. Non-uniform Braneworld Stars: An Exact Solution. *Int. J. Mod. Phys. D* **2009**, *18*, 837–852. [CrossRef]
23. Ovalle, J. The Schwarzschild's Braneworld Solution. *Mod. Phys. Lett. A* **2010**, *25*, 3323–3334. [CrossRef]

24. Casadio, R.; Ovalle, J. Brane-world stars and (microscopic) black holes. *Phys. Lett. B* **2012**, *715*, 251–255. [CrossRef]
25. Casadio, R.; Ovalle, J. Brane-world stars from minimal geometric deformation, and black holes. *Gen. Rel. Grav.* **2014**, *46*, 1669. [CrossRef]
26. Ovalle, J.; Gergely, L.Á.; Casadio, R. Brane-world stars with a solid crust and vacuum exterior. *Class. Quant. Grav.* **2015**, *32*, 045015. [CrossRef]
27. Ovalle, J. Decoupling gravitational sources in general relativity: The extended case. *Phys. Lett. B* **2019**, *788*, 213–218. [CrossRef]
28. Fernandes-Silva, A.; Ferreira-Martins, A.J.; da Rocha, R. Extended quantum portrait of MGD black holes and information entropy. *Phys. Lett. B* **2019**, *791*, 323–330. [CrossRef]
29. Herrera, L. New definition of complexity for self-gravitating fluid distributions: The spherically symmetric, static case. *Phys. Rev. D* **2018**, *97*, 044010. [CrossRef]
30. Abbas, G.; Nazar, H. Complexity factor for static anisotropic self-gravitating source in $f(R)$ gravity. *Eur. Phys. J. C* **2018**, *78*, 510. [CrossRef]
31. Sharif, M.; Butt, I.I. Complexity Factor for Charged Spherical System. *Eur. Phys. J. C* **2018**, *78*, 688. [CrossRef]
32. Abbas, G.; Nazar, H. Complexity Factor For Anisotropic Source in Non-minimal Coupling Metric $f(R)$ Gravity. *Eur. Phys. J. C* **2018**, *78*, 957. [CrossRef]
33. Nazar, H.; Abbas, G. Complexity factor for dynamical spherically symmetric fluid distributions in f(R) gravity. *Int. J. Geom. Meth. Mod. Phys.* **2019**, *16*, 1950170. [CrossRef]
34. Sharif, M.; Majid, A. Complexity factor for static sphere in self-interacting Brans–Dicke gravity. *Chin. J. Phys.* **2019**, *61*, 38–46. [CrossRef]
35. Sharif, M.; Majid, A.; Nasir, M.M.M. Complexity factor for self-gravitating system in modified Gauss–Bonnet gravity. *Int. J. Mod. Phys. A* **2019**, *34*, 1950210. [CrossRef]
36. Khan, S.; Mardan, S.A.; Rehman, M.A. Framework for generalized polytropes with complexity factor. *Eur. Phys. J. C* **2019**, *79*, 1037. [CrossRef]
37. Nazar, H.; Alkhaldi, A.H.; Abbas, G.; Shahzad, M.R. Complexity factor for anisotropic self-gravitating sphere in Rastall gravity. *Int. J. Mod. Phys. A* **2021**, *36*, 2150233. [CrossRef]
38. Arias, C.; Contreras, E.; Fuenmayor, E.; Ramos, A. Anisotropic star models in the context of vanishing complexity. *Ann. Phys.* **2022**, *436*, 168671. [CrossRef]
39. Rincon, A.; Panotopoulos, G.; Lopes, I. Anisotropic Quark Stars with an Interacting Quark Equation of State within the Complexity Factor Formalism. *Universe* **2023**, *9*, 72. [CrossRef]
40. Rincón, Á.; Panotopoulos, G.; Lopes, I. Anisotropic stars made of exotic matter within the complexity factor formalism. *Eur. Phys. J. C* **2023**, *83*, 116. [CrossRef]
41. Karmarkar, K.R. Gravitational metrics of spherical symmetry and class one. *Proc. Ind. Acad. Sci. A* **1948**, *27*, 56. [CrossRef]
42. Maurya, S.K.; Gupta, S.T.T.Y.K.; Rahaman, F. A new exact anisotropic solution of embedding class one. *Eur. Phys. J. A* **2016**, *52*, 191. [CrossRef]
43. Singh, K.N.; Bhar, P.; Pant, N. A new solution of embedding class I representing anisotropic fluid sphere in general relativity. *Int. J. Mod. Phys. D* **2016**, *25*, 1650099. [CrossRef]
44. Bhar, P.; Maurya, S.K.; Gupta, Y.K.; Manna, T. Modelling of anisotropic compact stars of embedding class one. *Eur. Phys. J. A* **2016**, *52*, 312. [CrossRef]
45. Maurya, S.K.; Gupta, Y.K.; Ray, S.; Deb, D. A new model for spherically symmetric charged compact stars of embedding class 1. *Eur. Phys. J. C* **2017**, *77*, 45. [CrossRef]
46. Bhar, P.; Govender, M. Anisotropic charged compact star of embedding class I. *Int. J. Mod. Phys. D* **2016**, *26*, 1750053. [CrossRef]
47. Maurya, S.K.; Maharaj, S.D. Anisotropic fluid spheres of embedding class one using Karmarkar condition. *Eur. Phys. J. C* **2017**, *77*, 328. [CrossRef]
48. Bhar, P.; Singh, K.N.; Manna, T. A new class of relativistic model of compact stars of embedding class I. *Int. J. Mod. Phys. D* **2017**, *26*, 1750090. [CrossRef]
49. Tello-Ortiz, F.; Maurya, S.K.; Errehymy, A.; Singh, K.N.; Daoud, M. Anisotropic relativistic fluid spheres: An embedding class I approach. *Eur. Phys. J. C* **2019**, *79*, 885. [CrossRef]
50. Jasim, M.K.; Maurya, S.K.; Al-Sawaii, A.S.M. A generalised embedding class one static solution describing anisotropic fluid sphere. *Astrophys. Space Sci.* **2020**, *365*, 9. [CrossRef]
51. Baskey, L.; Das, S.; Rahaman, F. An analytical anisotropic compact stellar model of embedding class I. *Mod. Phys. Lett. A* **2021**, *36*, 2150028. [CrossRef]
52. Zubair, M.; Waheed, S.; Javaid, H. A Generic Embedding Class-I Model via Karmarkar Condition in Gravity. *Adv. Astron.* **2021**, *2021*, 6685578. [CrossRef]
53. Demorest, P.; Pennucci, T.; Ransom, S.; Roberts, M.; Hessels, J. Shapiro Delay Measurement of A Two Solar Mass Neutron Star. *Nature* **2010**, *467*, 1081–1083. [CrossRef]

54. Antoniadis, J.; Freire, P.C.C.; Wex, N.; Tauris, T.M.; Lynch, R.S.; van Kerkwijk, M.H.; Kramer, M.; Bassa, C.; Dhillon, V.S.; Driebe, T.; et al. A Massive Pulsar in a Compact Relativistic Binary. *Science* **2013**, *340*, 6131. [CrossRef]
55. Sullivan, A.G.; Romani, R.W. A Joint X-ray and Optical Study of the Massive Redback Pulsar J2215+5135. *arXiv* **2024**, arXiv:2405.13889. [CrossRef]
56. Weber, F. Strange quark matter and compact stars. *Prog. Part. Nucl. Phys.* **2005**, *54*, 193–288. [CrossRef]
57. Aziz, A.; Ray, S.; Rahaman, F.; Khlopov, M.; Guha, B.K. Constraining values of bag constant for strange star candidates. *Int. J. Mod. Phys. D* **2019**, *28*, 1941006. [CrossRef]
58. Miller, M.C.; Lamb, F.K.; Dittmann, A.J.; Bogdanov, S.; Arzoumanian, Z.; Gendreau, K.C.; Guillot, S.; Ho, W.C.G.; Lattimer, J.M.; Loewenstein, M.; et al. The Radius of PSR J0740+6620 from NICER and XMM-Newton Data. *Astrophys. J. Lett.* **2021**, *918*, L28. [CrossRef]
59. Riley, T.E.; Watts, A.L.; Ray, P.S.; Bogdanov, S.; Guillot, S.; Morsink, S.M.; Bilous, A.V.; Arzoumanian, Z.; Choudhury, D.; Deneva, J.S.; et al. A NICER View of the Massive Pulsar PSR J0740+6620 Informed by Radio Timing and XMM-Newton Spectroscopy. *Astrophys. J. Lett.* **2021**, *918*, L27. [CrossRef]
60. Salmi, T.; Vinciguerra, S.; Choudhury, D.; Riley, T.E.; Watts, A.L.; Remillard, R.A.; Ray, P.S.; Bogdanov, S.; Guillot, S.; Arzoumanian, Z.; et al. The Radius of PSR J0740+6620 from NICER with NICER Background Estimates. *Astrophys. J.* **2022**, *941*, 150. [CrossRef]
61. Doroshenko, V.; Suleimanov, V.; Pühlhofer, G.; Santangelo, A. A strangely light neutron star within a supernova remnant. *Nat. Astron.* **2022**, *6*, 1444–1451. [CrossRef]
62. Sagun, V.; Giangrandi, E.; Dietrich, T.; Ivanytskyi, O.; Negreiros, R.; Providência, C. What Is the Nature of the HESS J1731-347 Compact Object? *Astrophys. J.* **2023**, *958*, 49. [CrossRef]
63. Brillante, A.; Mishustin, I.N. Radial oscillations of neutral and charged hybrid stars. *EPL* **2014**, *105*, 39001. [CrossRef]
64. Kokkotas, K.D.; Ruoff, J. Radial oscillations of relativistic stars. *Astron. Astrophys.* **2001**, *366*, 565. [CrossRef]
65. Miniutti, G.; Pons, J.A.; Berti, E.; Gualtieri, L.; Ferrari, V. Non-radial oscillation modes as a probe of density discontinuities in neutron stars. *Mon. Not. Roy. Astron. Soc.* **2003**, *338*, 389. [CrossRef]
66. Panotopoulos, G.; Lopes, I. Radial oscillations of strange quark stars admixed with condensed dark matter. *Phys. Rev. D* **2017**, *96*, 083013. [CrossRef]
67. Passamonti, A.; Bruni, M.; Gualtieri, L.; Nagar, A.; Sopuerta, C.F. Coupling of radial and axial non-radial oscillations of compact stars: Gravitational waves from first-order differential rotation. *Phys. Rev. D* **2006**, *73*, 084010. [CrossRef]
68. Passamonti, A.; Bruni, M.; Gualtieri, L.; Sopuerta, C.F. Coupling of radial and non-radial oscillations of relativistic stars: Gauge-invariant formalism. *Phys. Rev. D* **2005**, *71*, 024022. [CrossRef]
69. Savonije, G.J. Non-radial oscillations of the rapidly rotating Be star HD 163868. *Astron. Astrophys.* **2007**, *469*, 1057. [CrossRef]
70. Vásquez Flores, C.; Hall, Z.B., II; Jaikumar, P. Nonradial oscillation modes of compact stars with a crust. *Phys. Rev. C* **2017**, *96*, 065803. [CrossRef]
71. Flores, C.V.; Lugones, G. Radial oscillations of color superconducting self-bound quark stars. *Phys. Rev. D* **2010**, *82*, 063006. [CrossRef]
72. Franco, L.M.; Link, B.; Epstein, R.I. Quaking neutron stars. *Astrophys. J.* **2000**, *543*, 987. [CrossRef]
73. Andersson, N.; Jones, D.I.; Kokkotas, K.D.; Stergioulas, N. R mode runaway and rapidly rotating neutron stars. *Astrophys. J. Lett.* **2000**, *534*, L75. [CrossRef]
74. Tsang, D.; Read, J.S.; Hinderer, T.; Piro, A.L.; Bondarescu, R. Resonant Shattering of Neutron Star Crusts. *Phys. Rev. Lett.* **2012**, *108*, 011102. [CrossRef]
75. Chirenti, C.; Gold, R.; Miller, M.C. Gravitational waves from f-modes excited by the inspiral of highly eccentric neutron star binaries. *Astrophys. J.* **2017**, *837*, 67. [CrossRef]
76. Michel, E.; Baglin, A.; Auvergne, M.; Catala, C.; Samadi, R. CoRoT measures solar-like oscillations and granulation in stars hotter than the Sun. *Science* **2008**, *322*, 558–560. [CrossRef] [PubMed]
77. Mosser, B.; Belkacem, K.; Goupil, M.J.; Miglio, A.; Morel, T.; Barban, C.; Baudin, F.; Hekker, S.; Samadi, R.; Ridder, J.D.; et al. Red-giant seismic properties analyzed with CoRoT. *Astron. Astrophys.* **2010**, *517*, A22. [CrossRef]
78. Mosser, B.; Belkacem, K.; Goupil, M.J.; Michel, E.; Elsworth, Y.; Barban, C.; Kallinger, T.; Hekker, S.; DeRidder, J.; Samadi, R.; et al. The universal red-giant oscillation pattern: An automated determination with CoRoT data. *Astron. Astrophys.* **2011**, *525*, L9. [CrossRef]
79. Bischoff-Kim, A.; Østensen, R.H. Asteroseismology of the Kepler field DBV White Dwarf—It's a hot one! *Astrophys. J. Lett.* **2011**, *742*, L16. [CrossRef]
80. Evans, M.; Adhikari, R.X.; Afle, C.; Ballmer, S.W.; Biscoveanu, S.; Borhanian, S.; Brown, D.A.; Chen, Y.; Eisenstein, R.; Gruson, A.; et al. A Horizon Study for Cosmic Explorer: Science, Observatories, and Community. *arXiv* **2021**, arXiv:2109.09882.
81. Punturo, M.; Abernathy, M.; Acernese, F.; Allen, B.; Andersson, N.; Arun, K.; Barone, F.; Barr, B.; Barsuglia, M.; Beker, M.; et al. The Einstein Telescope: A third-generation gravitational wave observatory. *Class. Quant. Grav.* **2010**, *27*, 194002. [CrossRef]
82. Ovalle, J.; Linares, F. Tolman IV solution in the Randall-Sundrum Braneworld. *Phys. Rev. D* **2013**, *88*, 104026. [CrossRef]

83. Tolman, R.C. Static solutions of Einstein's field equations for spheres of fluid. *Phys. Rev.* **1939**, *55*, 364–373. [CrossRef]
84. Oppenheimer, J.R.; Volkoff, G.M. On massive neutron cores. *Phys. Rev.* **1939**, *55*, 374–381. [CrossRef]
85. Schwarzschild, K. On the gravitational field of a mass point according to Einstein's theory. *Sitzungsber. Preuss. Akad. Wiss. Berlin Math. Phys.* **1916**, *1916*, 189–196.
86. Barua, J.; Krori, K.D. A singularity-free solution for a charged fluid sphere in general relativity. *J. Phys. A* **1975**, *8*, 508.
87. Moustakidis, C.C. The stability of relativistic stars and the role of the adiabatic index. *Gen. Rel. Grav.* **2017**, *49*, 68. [CrossRef]
88. Hawking, S.W.; Ellis, G.F.R. *The Large Scale Structure of Space-Time*; Cambridge University Press: Chicago, UK, 2023.
89. Wald, R.M. *General Relativity*; Chicago University Press: Chicago, IL, USA, 1984.
90. Frolov, V.P.; Novikov, I.D. *Black Hole Physics: Basic Concepts and New Developments*; Springer: Berlin, Germany, 1998.
91. Panotopoulos, G.; Vernieri, D.; Lopes, I. Quark stars with isotropic matter in Hořava gravity and Einstein–æther theory. *Eur. Phys. J. C* **2020**, *80*, 537. [CrossRef]
92. Balart, L.; Panotopoulos, G.; Rincón, Á. Regular Charged Black Holes, Energy Conditions, and Quasinormal Modes. *Fortsch. Phys.* **2023**, *71*, 2300075. [CrossRef]
93. Gondek-Rosinska, D.; Limousin, F. The final phase of inspiral of strange quark star binaries. *arXiv* **2008**, arXiv:0801.4829.
94. Drago, A.; Lavagno, A.; Pagliara, G. Can very compact and very massive neutron stars both exist? *Phys. Rev. D* **2014**, *89*, 043014. [CrossRef]
95. Drago, A.; Lavagno, A.; Pagliara, G.; Pigato, D. The scenario of two families of compact stars: 1. Equations of state, mass-radius relations and binary systems. *Eur. Phys. J. A* **2016**, *52*, 40. [CrossRef]
96. Drago, A.; Pagliara, G. The scenario of two families of compact stars: 2. Transition from hadronic to quark matter and explosive phenomena. *Eur. Phys. J. A* **2016**, *52*, 41. [CrossRef]
97. Chanmugan, G. Radial oscillations of zero-temperature white dwarfs and neutron stars below nuclear densities. *ApJ* **1977**, *217*, 799. [CrossRef]
98. Väth, H.M.; Chanmugan, G. Radial oscillations of neutron stars and strange stars. *Astron. Astrophys.* **1992**, *260*, 250.
99. Arbañil, J.D.V.; Panotopoulos, G. Tidal deformability and radial oscillations of anisotropic polytropic spheres. *Phys. Rev. D* **2022**, *105*, 024008. [CrossRef]
100. Tassoul, M. Asymptotic approximations for stellar nonradial pulsations. *ApJS* **1980**, *43*, 469. [CrossRef]
101. Chaplin, W.J.; Miglio, A. Asteroseismology of Solar-Type and Red-Giant Stars. *Ann. Rev. Astron. Astrophys.* **2013**, *51*, 353. [CrossRef]
102. Capelo, D.; Lopes, I. The impact of composition choices on solar evolution: Age, helio- and asteroseismology, and neutrinos. *Mon. Not. Roy. Astron. Soc.* **2020**, *498*, 1992–2000. [CrossRef]
103. Panotopoulos, G. Stellar Modeling via the Tolman IV Solution: The Cases of the Massive Pulsar J0740+6620 and the HESS J1731-347 Compact Object. *Universe* **2024**, *10*, 342. [CrossRef]
104. Raaijmakers, G.; Greif, S.K.; Hebeler, K.; Hinderer, T.; Nissanke, S.; Schwenk, A.; Riley, T.E.; Watts, A.L.; Lattimer, J.M.; Ho, W.C.G. Constraints on the Dense Matter Equation of State and Neutron Star Properties from NICER's Mass–Radius Estimate of PSR J0740+6620 and Multimessenger Observations. *Astrophys. J. Lett.* **2021**, *918*, L29. [CrossRef]
105. Pang, P.T.H.; Tews, I.; Coughlin, M.W.; Bulla, M.; Broeck, C.V.D.; Dietrich, T. Nuclear Physics Multimessenger Astrophysics Constraints on the Neutron Star Equation of State: Adding NICER's PSR J0740+6620 Measurement. *Astrophys. J.* **2021**, *922*, 14. [CrossRef]
106. Ascenzi, S.; Graber, V.; Rea, N. Neutron-star measurements in the multi-messenger Era. *Astropart. Phys.* **2024**, *158*, 102935. [CrossRef]

Disclaimer/Publisher's Note: The statements, opinions and data contained in all publications are solely those of the individual author(s) and contributor(s) and not of MDPI and/or the editor(s). MDPI and/or the editor(s) disclaim responsibility for any injury to people or property resulting from any ideas, methods, instructions or products referred to in the content.